












A wireless, implantable bioelectronic system for monitoring urinary bladder function following surgical recovery

Jihye Kim^{a,b,1} , Matthew I. Bury^{c,d,1}, Kyeongha Kwon^{e,1}, Jae-Young Yoo^{a,f}, Nadia V. Halstead^c, Hee-Sup Shin^a , Shupeng Li^g , Sang Min Won^h, Min-Ho Seoⁱ, Yunyun Wu^g, Do Yun Park^e, Mitali Kini^j, Jean Won Kwak^g, Surabhi R. Madhvapathy^g, Joanna L. Ciatti^g, Jae Hee Lee^a, Suyeon Kim^a, Hanjun Ryu^{a,k}, Kento Yamagishi^g, Hong-Joon Yoon^{a,l} , Sung Soo Kwak^{a,m} , Bosung Kim^g, Yonggang Huang^{a,g} , Lisa C. Hallidayⁿ, Earl Y. Cheng^{c,j}, Guillermo A. Ameer^{a,o,p,q,r,s,t,2} , Arun K. Sharma^{c,d,j,o,p,u,2} , and John A. Rogers^{a,g,o,p,q,r,s,t,v,w,2} 

Contributed by John A. Rogers; received January 15, 2024; accepted February 25, 2024; reviewed by Hatim Thaker and Sheng Xu

Partial cystectomy procedures for urinary bladder–related dysfunction involve long recovery periods, during which urodynamic studies (UDS) intermittently assess lower urinary tract function. However, UDS are not patient-friendly, they exhibit user-to-user variability, and they amount to snapshots in time, limiting the ability to collect continuous, longitudinal data. These procedures also pose the risk of catheter-associated urinary tract infections, which can progress to ascending pyelonephritis due to prolonged lower tract manipulation in high-risk patients. Here, we introduce a fully bladder-implantable platform that allows for continuous, real-time measurements of changes in mechanical strain associated with bladder filling and emptying via wireless telemetry, including a wireless bioresorbable strain gauge validated in a benchtop partial cystectomy model. We demonstrate that this system can reproducibly measure real-time changes in a rodent model up to 30 d postimplantation with minimal foreign body response. Studies in a nonhuman primate partial cystectomy model demonstrate concordance of pressure measurements up to 8 wk compared with traditional UDS. These results suggest that our system can be used as a suitable alternative to UDS for long-term postoperative bladder recovery monitoring.

bladder | regeneration | bioelectronics | wireless | sensing

The urinary bladder is a hollow organ that expands and contracts to allow for the storage and emptying of urine during micturition under volitional control (1–3). Patients who are candidates for a bladder-sparing treatment approach for muscle-invasive bladder cancer may undergo a partial cystectomy, while those with end-stage neurogenic bladder will be offered bladder augmentation enterocystoplasty (4–7). In these patients, complete functional recovery of bladder mechanics following surgical excision of the bladder wall is typically slow and difficult to assess. Urodynamic studies (UDS) are essential in the diagnosis and management of lower urinary tract dysfunction in the pre- and postoperative settings. Abnormal or worsening urodynamic parameters, such as high bladder storage pressures and decreased bladder capacity, can be symptomatic of impending upper urinary tract deterioration and subsequent renal failure (8, 9). In the clinical setting, UDS involve inserting urethral catheters and rectal electromyography electrodes, filling the bladder with saline at a set rate, and measuring changes in detrusor pressures during filling and emptying cycles. These measurements are correlated with patient symptoms to aid in diagnosis. This office-based procedure is often time consuming, expensive, and results in significant patient discomfort. Traditional urodynamics can be limited by non-diagnostic results due to patient intolerance, or poor interrater reliability and protocol inconsistency due to variations in provider training (8, 9). Additionally, these studies only provide a glimpse into bladder function at a single point in time and do not reflect the characteristics of chronic urinary conditions that many patients face, particularly with ambulation and daily activities.

To improve upon the accessibility and to address the diagnostic limitations of urodynamics, there is growing interest in ambulatory urodynamic monitoring (AUM) with continuous catheter-based pressure sensing (8, 10). These studies suggest that AUM could replace conventional office urodynamics with portable recording devices that have the potential to detect involuntary detrusor activity with improved specificity. The use of chronic catheterization can, however, lead to stone formation, significant patient discomfort, and risk for urinary tract infections with ascending pyelonephritis. Recent technological advances form the basis of implantable, soft, and stretchable electronic bladder pressure sensors with the ability to obtain long-term, continuous data on bladder storage and emptying parameters without the use of indwelling catheters. These devices

Significance

Increasing interest in personalized medical systems motivates the development of bioelectronic implants for sensing physiological functions. Such implants could potentially provide physicians with real-time information to guide treatment and management strategies regarding tissue disease or trauma. Within the context of urinary bladder dysfunction, internal pressures can be indicative of bladder recovery following surgical interventions. This study reports a fully implantable system for quantitative measurements of the temporal dynamics of bladder filling and voiding via wireless telemetry, employing stretchable strain gauges in both permanent and bioresorbable forms. Validation studies in rodent and nonhuman primate models demonstrate the potential for this system to provide personalized treatment and rehabilitation strategies to human counterparts.

Reviewers: H.T., Boston Children's Hospital; and S.X., University of California at San Diego.

The authors declare no competing interest.

Copyright © 2024 the Author(s). Published by PNAS. This article is distributed under [Creative Commons Attribution-NonCommercial-NoDerivatives License 4.0 \(CC BY-NC-ND\)](https://creativecommons.org/licenses/by-nc-nd/4.0/).

¹J.K., M.I.B., and K.K. contributed equally to this work.

²To whom correspondence may be addressed. Email: g-ameer@northwestern.edu, arun-sharma@northwestern.edu, or jrogers@northwestern.edu.

This article contains supporting information online at <https://www.pnas.org/lookup/suppl/doi:10.1073/pnas.2400868121/-/DCSupplemental>.

Published March 28, 2024.

come in the forms of intravesical, intradetrusor, or transdetrusor platforms. Many are limited by short battery lives, limited operational range, and/or requirements for explantation and disassembly to retrieve data (8, 10). Majerus et al. describe the use of a wireless implantable intracavity micromanometer (WIMM), a battery-powered rechargeable device that permanently implants cystoscopically within the wall of the bladder. The data from this study demonstrate adequate wireless detection of pressure changes in real-time and a correlation coefficient of $r = 0.95$ with a matched reference device when used in anesthetized female canine subjects (11). Additionally, this study suggests potential applications in a “closed-loop system” by relaying feedback to coupled neuromodulation devices. The experimental prototype is, however, bulky, with a battery life of 1 wk with need for intermittent recharge sessions, given that it is a permanently implanted device (11). In 2017, the same group published data on the suburothelial implantation of their piezoelectric catheter-free pressure sensor in a canine model. The results show a strong correlation ($r = 0.98$) between the device and reference catheter data in these animal subjects. Limitations are in the use of a wired prototype and the loss of consistent recordings due to significant erosion of the implant through the detrusor in the majority of the subjects (12). Frainey et al published their data using the UroMonitor™ transurethral telemetric ambulatory pressure monitoring system in 11 human subjects (13). This monitoring system detects intravesical bladder pressure during a single office visit, with same-day reference measurements obtained by traditional UDS. While the authors demonstrate the feasibility of this approach and moderate correlation with UDS, the absence of long-term data prevents conclusions on safety and efficacy. Additionally, as an intravesical device, static pressure accuracy at low volumes is poorly correlative. Of note, the device is not designed to provide bladder volume data, thereby limiting the accuracy of compliance and capacity assessment (13). Previous work describes noninvasive bladder monitoring methods based on electrical impedance and ultrasound (14, 15). These techniques, however, are currently designed to monitor overall volume changes in the bladder, an averaged quantity. Detailed measurements of two or more different regions of a single bladder are difficult. Also, artifacts associated with body movements place constraints on measurement conditions. This consideration, along with the required wired hardware and external data acquisition equipment, makes long-term, real-time monitoring of volume changes impossible. Monitoring must therefore be performed episodically, in specialized facilities where equipment is installed, such as hospitals, resulting in additional medical costs and time/space constraints.

To avoid limitations associated with previously described monitoring platforms, we introduce here an implantable system that includes a strain gauge capable of real-time bladder monitoring via telemetry, with options in permanent as well as bioresorbable forms. The work includes rigorous experimental testing and computational modeling in benchtop phantoms of bladder insult/recovery as well as studies evaluating efficacy in rodent and non-human primate baboon injury models. Data accrued from these studies demonstrate an ability to monitor bladder pressure as a function of strain for extended periods of time via wireless, remote data capture and analysis. Although the overall risks of surgery for strain gauge implantation and removal are higher than those associated with pacing a chronic catheter, the system provides accurate measures of bladder strain compared to catheter placed intraluminally. Additionally, our technology reduces the risk of urinary tract infection compared to chronic catheterization and

offers the potential for a more comfortable solution for long-term monitoring.

Results

Bladder Function Monitoring System for Human Applications.

Fig. 1A shows a schematic illustration of the technology and envisioned clinical use case. Following a partial bladder cystectomy, the system continuously monitors filling and voiding dynamics through a soft, stretchable strain gauge that encircles the bladder and a companion wireless module that streams data to an external device using standard Bluetooth Low Energy (BLE) communication protocols. The resulting information provides insights to aid in care decisions associated with postoperative recovery and healing, potential complications due to infections, and other processes. Fig. 1B and *SI Appendix, Fig. S1*, present schematic illustrations and a photograph of the strain gauge and its helical interconnection to the wireless base station, respectively. A critical feature of the gauge is that it avoids any significant mechanical constraint on the natural processes of filling and voiding of the bladder, through the use of ultrathin, low modulus designs. The device exploits a silicone elastomer with low cross-linking density (Ecoflex 00-30), with a sensing region that contains particles of conducting carbon at loading levels slightly above the threshold for percolation electrical transport (16–18). The system can be designed as either a permanent implant for chronic monitoring or as a temporary device based on bioresorbable materials, specifically on poly(octamethylenemaleate (anhydride) citrate) (POMaC) and tungsten (W) particles (19–22). In this latter iteration, the strain gauge dissolves and disappears in the body to eliminate device load on the bladder after a period of clinical need (Fig. 1C). Fig. 1D shows the relative change in resistance of such a bioresorbable strain gauge following injection of saline into a bladder mimic at three different rates. Fig. 1E and *SI Appendix, Fig. S2*, illustrate the process of accelerated dissolution in phosphate-buffered saline (PBS, pH = 7.4) at 75 °C. The focus of the following description is on the permanent version of the device.

Strain Gauge Design and Assessment. A robust sensor with suitable properties follows from appropriate selection of the length of the sensing region, the thickness of the encapsulation (Ecoflex 00-30) at the interface to the helical wire, and the parameters for corona treatment of this interface to ensure robust adhesion. Increasing the length of the sensing region increases the relative change in resistance for a given strain (and thus the gauge factor), to levels that ensure high signal-to-noise ratio across a range of elongations relevant to filling and voiding of the bladder (*SI Appendix, Fig. S3A*). A thick encapsulation layer reduces the effects of artifacts due to motion of the wire relative to the gauge (*SI Appendix, Fig. S3B*). Specifically, increasing the thickness from ~100 to ~500 μm , decreases artifacts associated with shaking the wire from ~14% to ~3%. A balancing consideration is that thin encapsulation layers reduce the mechanical load on the bladder and the foreign body response. Results described in the following use a thickness of 500 μm . Finally, corona treatment of the connection area between the carbon black doped silicone elastomer and copper/polyimide (Cu/PI) electrodes ensures robust adhesion and long-term operation stability. *SI Appendix, Fig. S3C*, shows the results of cyclic bending tests to verify the long-term operation. Without corona treatment, the connection area between the carbon black doped

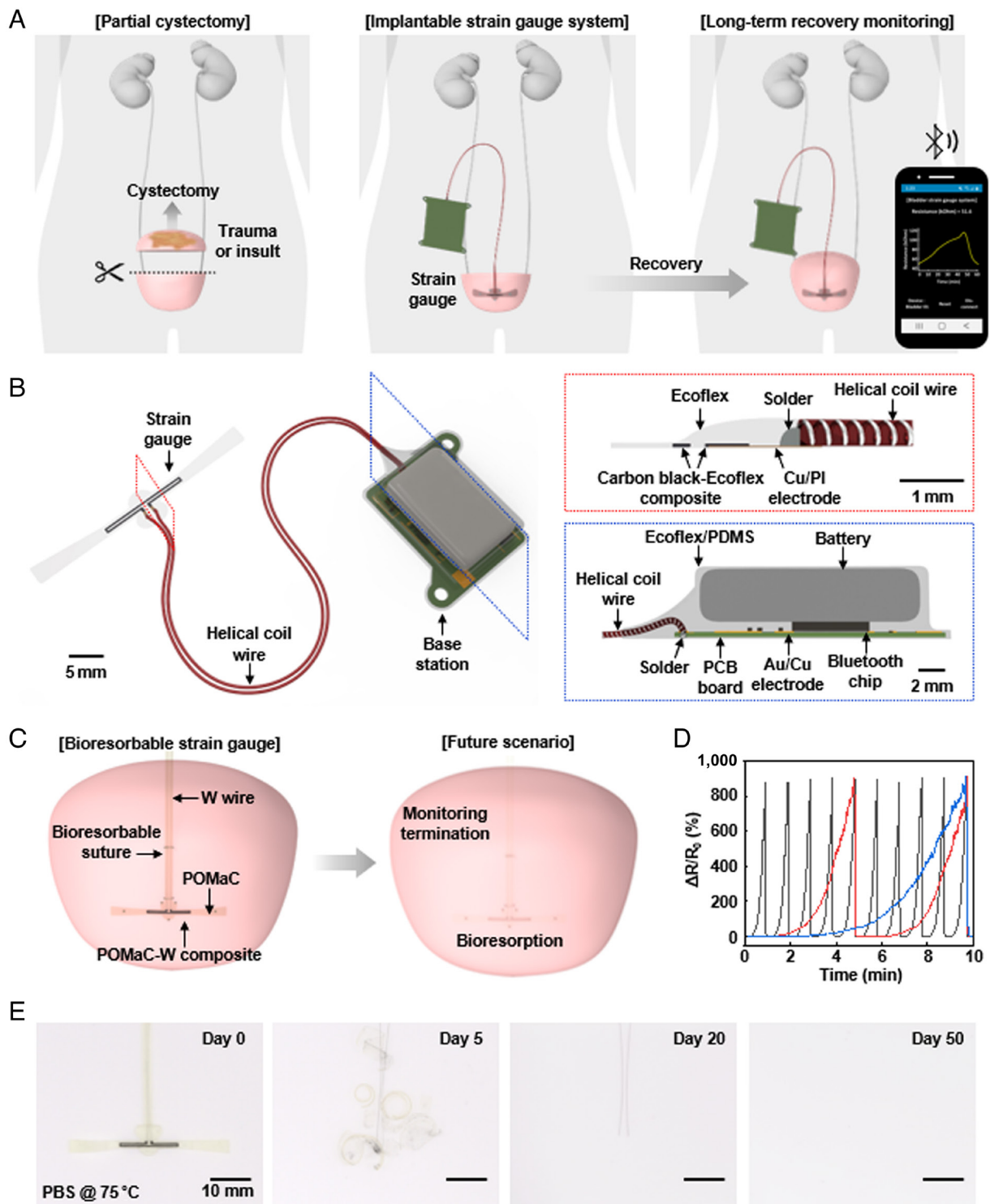


Fig. 1. Wireless implantable system for real-time, quantitative monitoring of bladder function. (A) Schematic illustration of the use scenario in long-term monitoring of the recovery and regeneration period after a partial cystectomy. (B) Schematic illustrations of the bladder monitoring system. (C) Illustration of the use of a bioresorbable strain gauge as the basis for a temporary monitoring system. (D) Relative change in resistance of a bioresorbable strain gauge due to filling of a mimic bladder at three different rates (black, red and blue line for 300, 60, 30 mL/min, respectively). (E) Images of the accelerated dissolution of a bioresorbable strain gauge in PBS solution (pH = 7.4) at 75 °C.

silicone elastomer and Cu/PI electrodes breaks after 45 cycles. With corona treatment, the connection area persists even beyond 25,000 cycles. Similar cyclic testing with different types of wires indicates that helical coils of stainless steel offer the best performance (*SI Appendix, Fig. S4*). *SI Appendix, Fig. S5*, shows a benchtop setup for comprehensive testing of the strain gauge and connecting wire using a silicone (Ecoflex 00-50; 260 kPa)

bladder mimic for a rat model (ellipsoid, 4.5 mm × 7.5 mm; 300 μm thickness) immersed in phosphate-buffered saline (PBS) solution at 37 °C. *SI Appendix, Fig. S6 A and B*, highlights the relative change in resistance as a function of the volume of saline injected into the bladder at three different rates. *SI Appendix, Fig. S6C*, shows the results of cyclic testing using this setup for over 100 h.

The helical coil wire serves as a connection to the base station, which consists of a printed circuit board (PCB), lithium-ion battery (60 mAh), and electronic components for measurement and digitalization of the resistance of the strain gauge and for wireless data transmission. Layers of parylene, marine epoxy and poly(dimethylsiloxane) (PDMS) encapsulate the base station to prevent penetration of biofluids and to establish a mechanically soft interface to surrounding tissues. *SI Appendix, Figs. S7 and S8*, summarizes the processes for fabricating the system.

Benchtop Validation in an Artificial Human Bladder Model.

The ultimate goal of this system is to monitor the degree of bladder recovery after partial cystectomy in patients with bladder trauma or injury and after suturing the excised bladder area with a bioresorbable scaffold (Fig. 2A). Benchtop studies using three models serve to verify the feasibility of this mode of use. The first model corresponds to the case after suturing the scaffold to the upper part of the resected bladder, with normal bladder tissue in

the lower part. The second corresponds to partial regeneration of bladder tissue with the scaffold. The third corresponds to fully regenerated bladder tissue and complete bioresorption of the scaffold. The mimic human bladder for these studies (ellipsoid, 45 mm × 50 mm) uses silicone materials with moduli comparable to normal human bladder tissue (Ecoflex 00-50, 260 kPa), tissue undergoing regeneration with the scaffold (Dragon Skin 10, 330 kPa) and the scaffold itself (Dragon Skin 20, 400 kPa), as summarized in Fig. 2B (23, 24). Simulations based on the finite element method (FEM) include the bladder and the strain gauges (*SI Appendix, Fig. S9 A–C*), for purposes of comparison to experimental results obtained with strain gauges on the upper (gauge A) and lower (gauge B) parts, for the case of injecting 300 mL of saline into the mimic bladders (*SI Appendix, Table S1*). In the first model (Fig. 2C), the lower normal bladder tissue expands more than the upper scaffold, as expected and as consistent with the responses of the strain gauges. In the second (Fig. 2D), these differences decrease, again as expected. In the third (Fig. 2E),

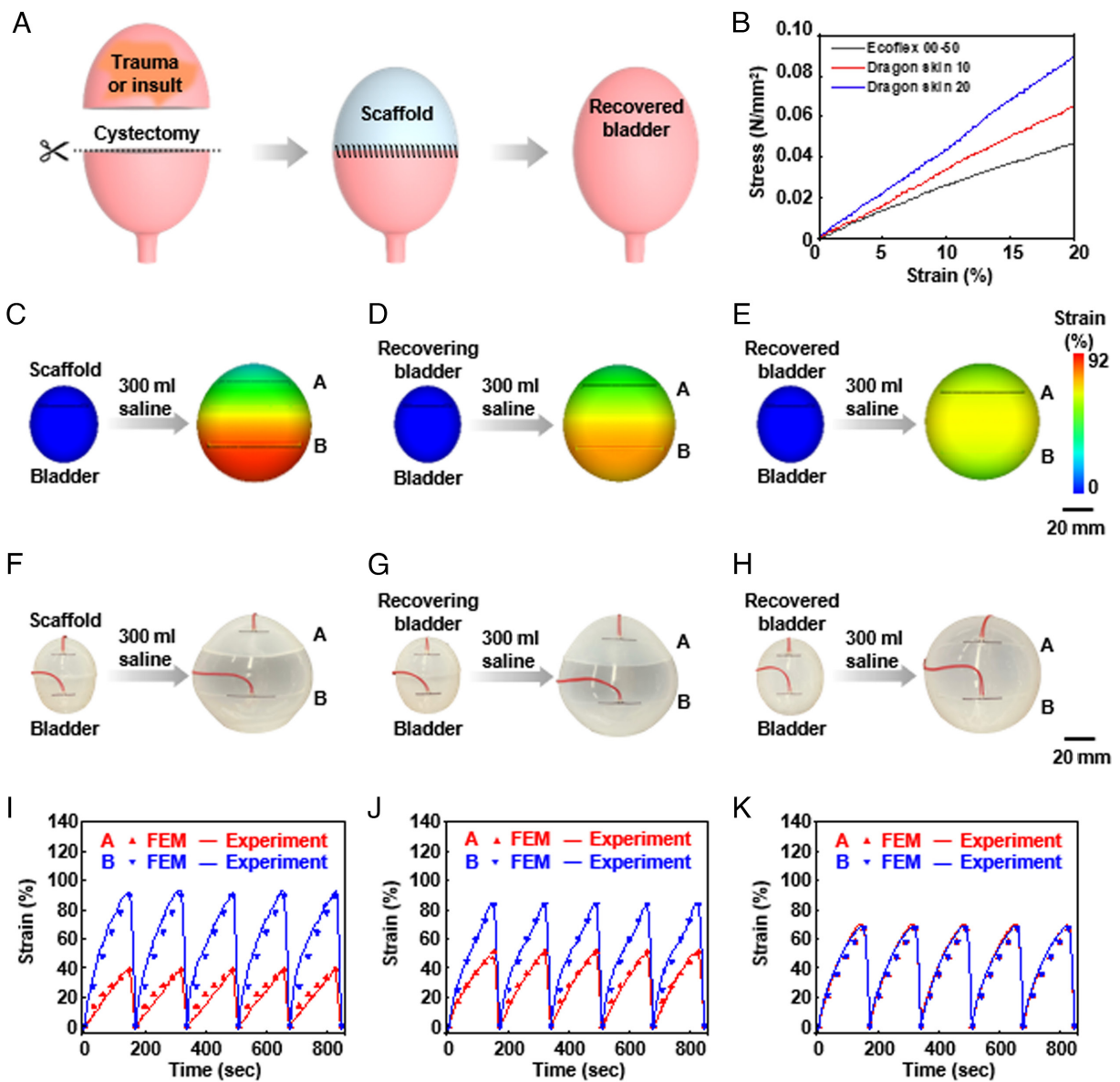


Fig. 2. Benchtop tests and FEM simulation results for monitoring of a human bladder model at three time points after a partial cystectomy (A) Schematic illustration of the recovery process with a scaffold implanted after a partial cystectomy. (B) Strain-stress curves of model materials for a normal bladder, a regenerating bladder on a scaffold, and a scaffold. (C–E) Strain distributions calculated from FEM simulations for three models after partial cystectomy and scaffold implantation. (F–K) Benchtop setups and strain changes for three models after partial cystectomy and scaffold implantation.

the fully regenerated upper bladder tissue and the lower normal bladder tissue show similar behaviors. Benchtop experimental results appear in Fig. 2 *F–H*. Converting the measured changes in resistance to strain allows direct comparisons of experiment to simulation, as summarized in Fig. 2 *I–K* and *SI Appendix, Fig. S3A*. In all cases, the findings are in good agreement, thereby establishing the use of the technologies introduced here for monitoring of bladder dynamics during recovery and regeneration after a cystectomy.

In Vivo Validation in a Rodent Model. Validation studies before testing in nonhuman primates involve rat models and surgical procedures for suturing the base station to the abdominal wall and the strain gauge to the bladder wall (Fig. 3 *A–C* and *SI Appendix, Fig. S10*). X-ray images at 2 and 4 wk postsurgery indicate that these schemes ensure stable positioning (*SI Appendix, Fig. S11*). As shown in Fig. 3 *D* and *E*, the resistance of the strain gauge gradually increases as urine fills

the bladder, and then decreases sharply as voiding occurs. Even with small levels of noise caused by movements of the body or organs, the system accurately detects both large (~1,300 μL) and small (~500 μL) voiding events, as validated by using filter paper assays (Fig. 3 *F* and *G* and *SI Appendix, Supporting Text and Figs. S12* and *S13*). *SI Appendix, Fig. S14*, presents the results of bladder tissue dissections at 7 d ($n = 3$), 14 d ($n = 3$), and 30 d ($n = 4$) postsurgery. Gross histological examination at 7 d reveals a minor foreign body response (FBR), with inflammatory tissue surrounding the strain gauge. The FBR persists at 14 and 30 d but with no increase in severity. Histology using hematoxylin and eosin (H&E) staining confirms this inflammatory response (*SI Appendix, Fig. S14 A–C*). *SI Appendix, Fig. S14 D–I*, shows the results of immunofluorescent staining with CD68 (macrophage marker) and MPO (myeloperoxidase, neutrophil marker) as key inflammatory markers. Initial quantification of CD68 proximal to the strain gauge at 7 d displays a positive rate of $15.6 \pm 5.9\%$. This value decreases to $12.0 \pm 2.0\%$ at 14 d and

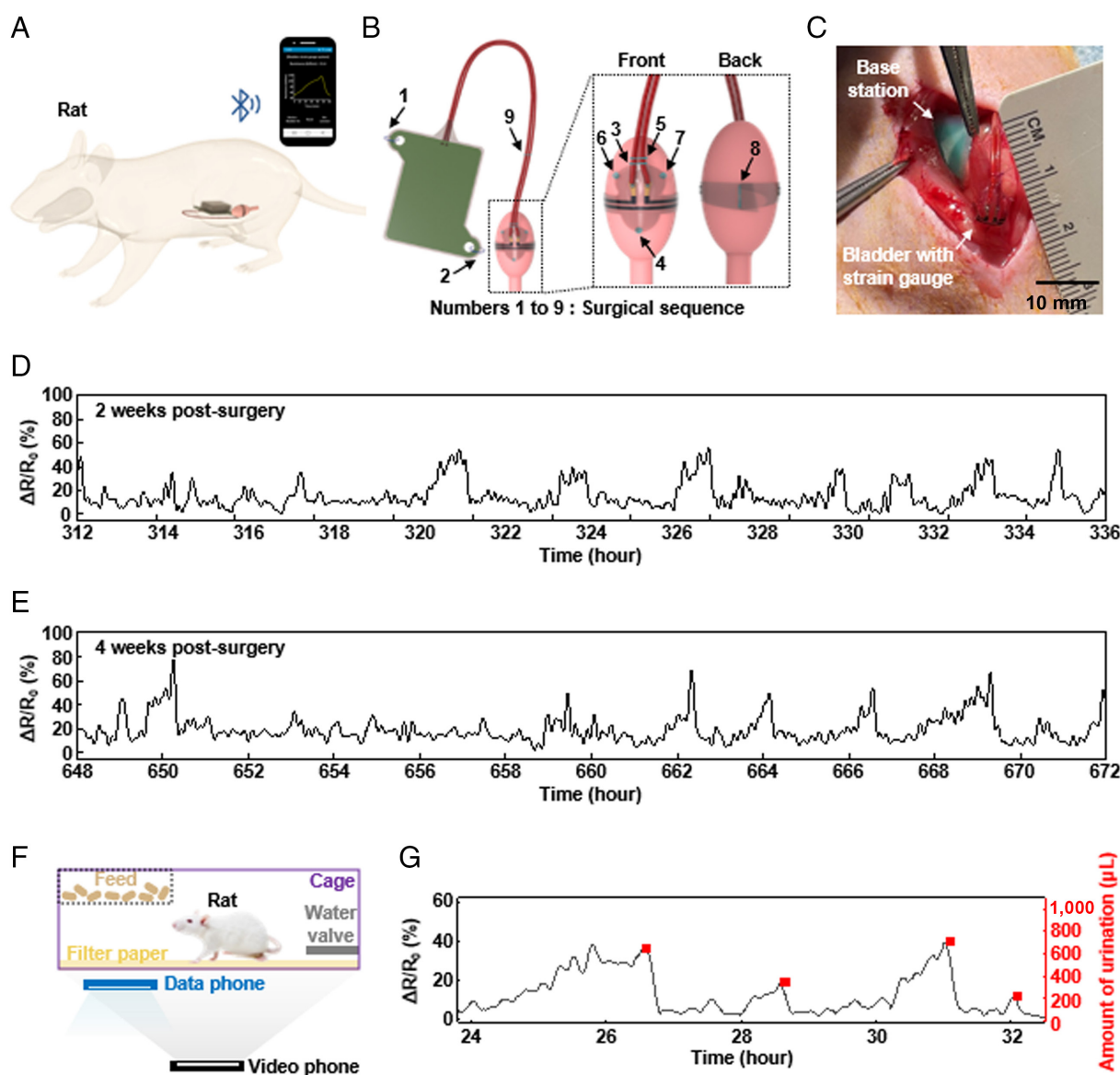


Fig. 3. (A) Schematic illustration of experiments with a rat model. (B) Illustrations of the system components, the positions of the suture holes, and interface to the bladder. (C) Photograph showing the strain gauge sutured onto the outside surface on the bladder wall of a rat. (D and E) Chronic measurements from a rat model. Relative change in resistance of the strain gauge as a function of time at 2 and 4 wk postsurgery. (F) Urine volume validation setup in a rat model. (G) Plot of the relative change in resistance of the strain gauge as a function of time (black) and amount of urine determined using the filter paper method (red).

then $6.8 \pm 2.6\%$ at 30 d. Initial quantification of MPO proximal to the strain gauge shows $5.9 \pm 1.6\%$ at 7 d, $2.6 \pm 0.6\%$ at 14 d, and $2.6 \pm 1.4\%$ at 30 d. *SI Appendix, Fig. S14J*, indicates that the FBR couples with an acute inflammatory response of both CD68 and MPO⁺ at 7 to 14 d but slowly subsides over the 30-d period.

UDS in a Nonhuman Primate Model. Fig. 4*A* illustrates the placement and use of the system in a nonhuman primate model (baboon), with the strain gauge sutured to the bladder wall. Four suture holes on the base station provide fixation to the abdominal wall (25). Fig. 4*B* illustrates the arrangement. Fig. 4*C* shows a photograph of the gauge after implantation. UDS involves insertion of a Foley catheter into the urethra for injection of contrast solution into the bladder using an instillation pump. During this process, a physiological pressure transducer measures the bladder pressure and C-arm fluoroscopy captures images

of the bladder and the strain gauge system. All urodynamics measurements use a consistent flow rate of approximately 10% of the bladder capacity, stopped at 20 cm H₂O intravesical pressure to minimize the potential for perforation of the bladder. The original bladder capacity of 95 mL (*SI Appendix, Fig. S15*) decreases to 60 mL (37% of original capacity) by 6 wk postsurgery but recovers to 82 mL (85.2% of original capacity) by 10 wk (*SI Appendix, Figs. S16 and S17*). This behavior likely follows from bladder instability during the postoperative recovery process rather than effects of the strain gauge implantation. For an animal with ~50% partial cystectomy, the volume decreases from 142 mL to 41 mL (28% of original capacity) by 6 wk postsurgery (*SI Appendix, Figs. S18 and S19*). Observations reveal no signs of detrusor overactivity (DO) in either animal across all time points. Ultrasound inspection fails to detect any hydronephrosis or hydroureter, and images of the bladder show a normal morphology. The Doppler images with corresponding

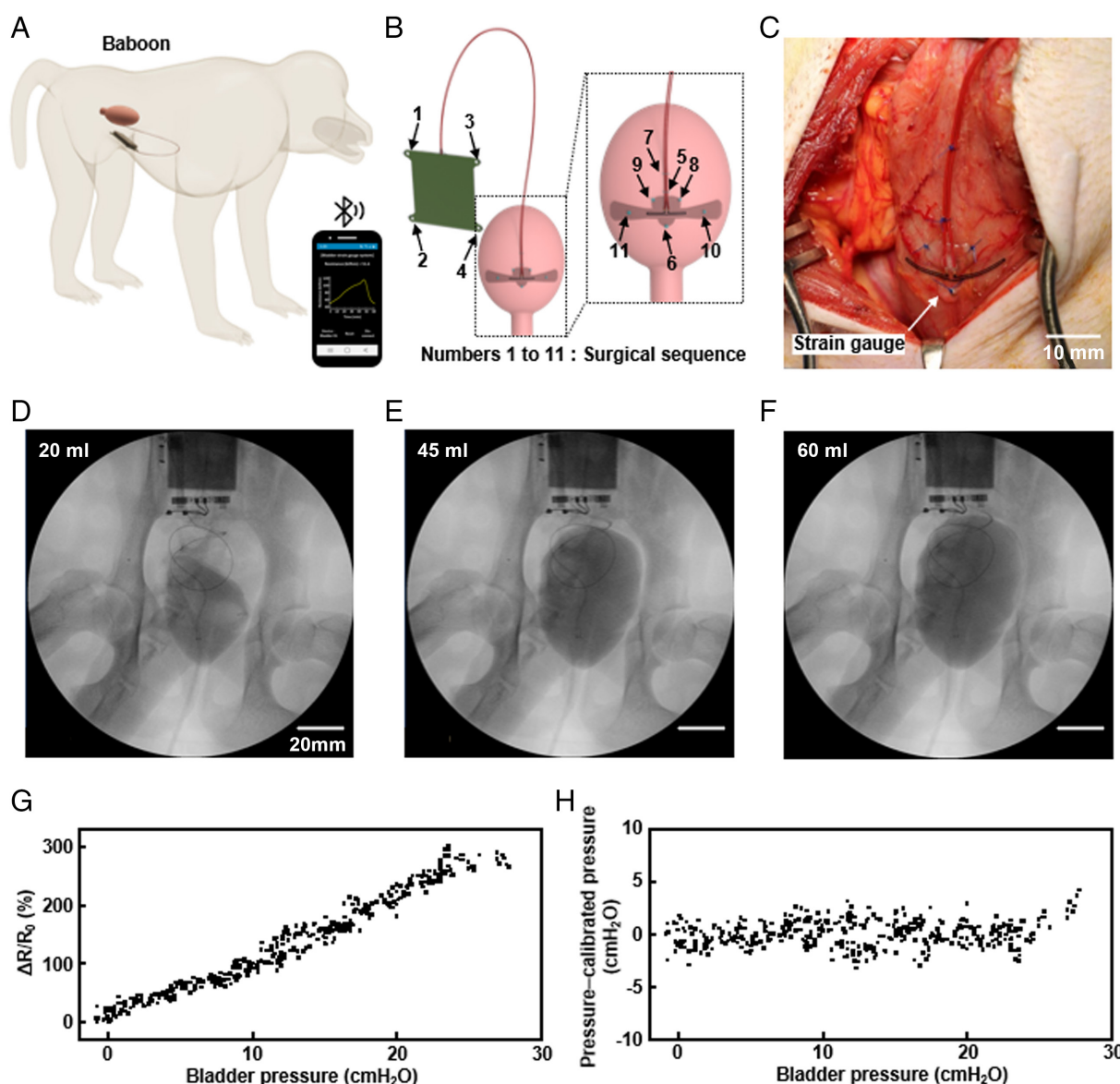


Fig. 4. Schematic illustrations and UDS for nonhuman primate models. (A) Diagrams of the location of the implanted system and BLE wireless interface to a smartphone. (B) Illustrations of the system components, the positions of the suture holes, and interface to the bladder. (C) Image of a strain gauge sutured to the surface of the bladder wall of a baboon with a normal bladder. (D–F) C-arm fluoroscopy images of UDS 6-wk post-surgery. (G) Plot of the relative change in resistance of the strain gauge as a function of the bladder pressure determined during a urodynamic study. (H) Bland–Altman plot, showing the difference between the pressure inferred from the strain gauge and that measured directly as a function of the latter.

spectra (*SI Appendix, Figs. S15–S19*) show no deleterious effects on kidney parenchyma with the implementation of the strain gauge. Fig. 4 *D–F* presents C-arm fluoroscopic images for the animal with a normal bladder after injection of 20, 45, and 60 mL of contrast solution. The solution first fills the lower part of the bladder and then expands the entire bladder wall. Placement of the strain gauge on this lower part thus facilitates detection

of even small amounts of urine. Calibration of the implanted strain gauge system involves measurements of changes in bladder pressure according to the volume of saline injected into the bladder through UDS, simultaneous with measurements of the relative change in resistance of the strain gauge. Fig. 4*G* presents a graph of the relative change in resistance of the strain gauge as a function of bladder pressure, showing a linear relationship as

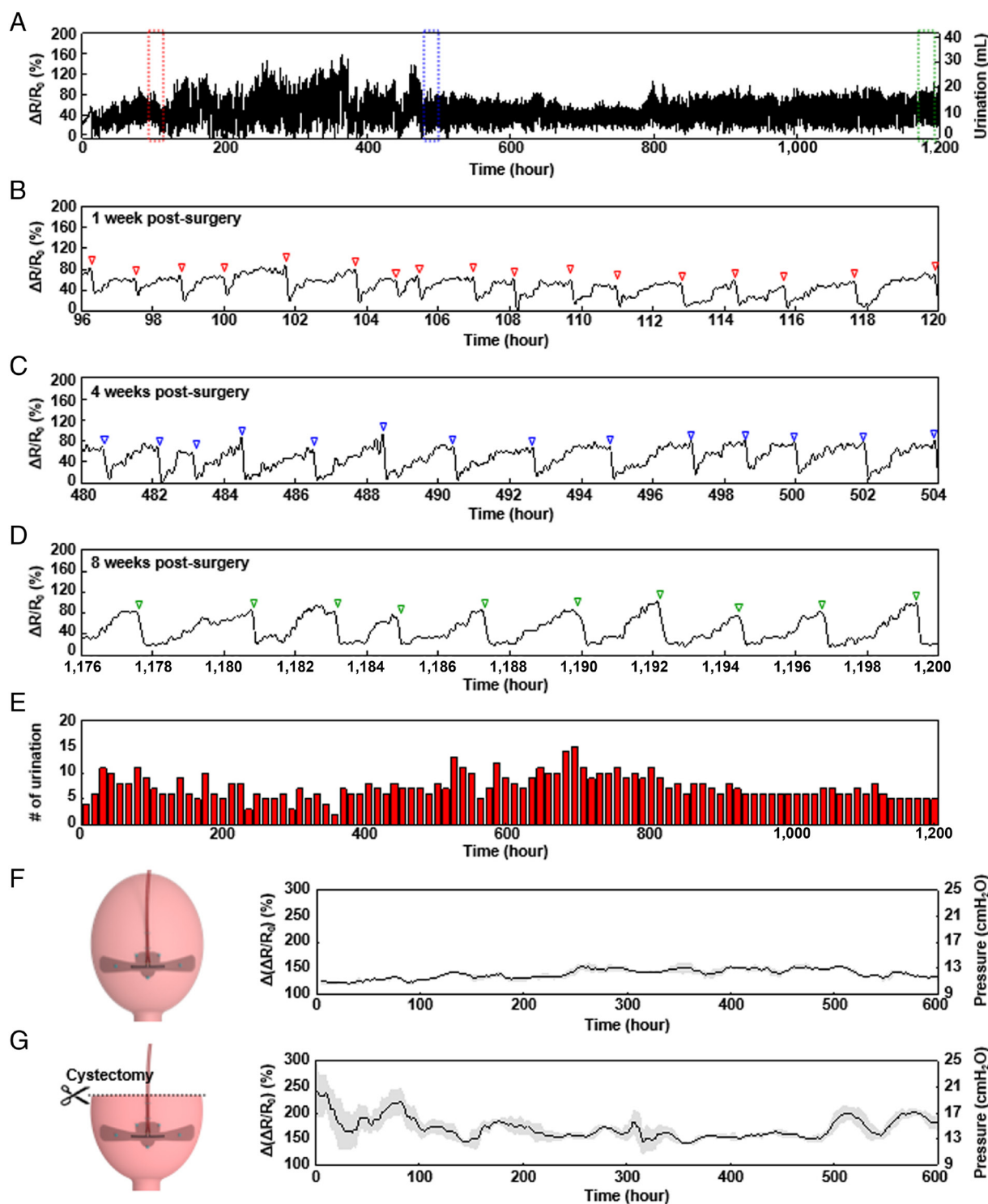


Fig. 5. Chronic studies in nonhuman primate models. (A) Relative change in the resistance of the strain gauge for the entire time period of the study. (B) Relative change in the resistance of the strain gauge at 1 wk postsurgery. (C) Relative change in the resistance of the strain gauge at 4 wk postsurgery. (D) Relative change in the resistance of the strain gauge at 8 wk postsurgery. (E) Number of voids in 12-h periods throughout the study. (F) Difference in resistance before and after voiding for an animal with a normal bladder. (G) Difference in resistance before and after voiding for an animal with a partial cystectomy.

expected. The Bland–Altman plot in Fig. 4H indicates that the average difference and the SD of bladder pressure inferred from the strain gauge and measured directly are 8.1×10^{-9} cmH₂O and -1.2 cmH₂O. Reproducible, long-term, and continuous measurements of pressure and volume changes provide aggregate data to the clinician in real-time, which can be used to determine immediate or longitudinal course of action when necessary.

Long-Term Strain Gauge Assessment in a Nonhuman Primate Model. Fig. 5 A–D summarizes wireless measurements in the nonhuman primate model for the entire period of the study and for 1, 4, and 8 wk postsurgery, respectively (SI Appendix, Figs. S20–S30). The capacity of the battery in the base station (500 mAh) is the only factor that limits the duration of data collection. The relative change in resistance of the strain gauge slowly increases as urine gradually accumulates into the bladder, and then decreases rapidly as voiding occurs, with good signal-to-noise in the ambulatory animal. Fig. 5 B–D shows minor motion artifacts caused by movements of the body and organs. Fig. 5E shows the number of voids over periods of 12 h, inferred from these data. The data indicate that this number fluctuates during

the first 6 wk before subsequently stabilizing to a consistent value, consistent with expected times for full recovery. SI Appendix, Fig. S31 A and B, highlights the times for filling and voiding of the bladder, respectively, as additional factors related to the degree of recovery. To compare the postoperative bladder activity between an animal with a normal bladder and one with a partial cystectomy (approximately 50%), Fig. 5 F and G presents differences in resistance before and after voiding for these two cases, respectively. The difference in resistance before and after voiding can be converted to the corresponding difference in bladder pressure based on the results of the urodynamics study (Fig. 4G). Compared to the normal bladder, the bladder with partial cystectomy shows a higher difference in resistance (strain), and therefore bladder pressure, before and after voiding. This expected result follows from the reduction in overall bladder capacity and the necessity to expand to a greater degree than a normal bladder to hold the same amount of urine. SI Appendix, Fig. S32, presents results of a confirming benchtop experiment. These findings, combined with the studies summarized in Fig. 2 strongly suggest applicability of this technology in monitoring recovery associated with a partial cystectomy.

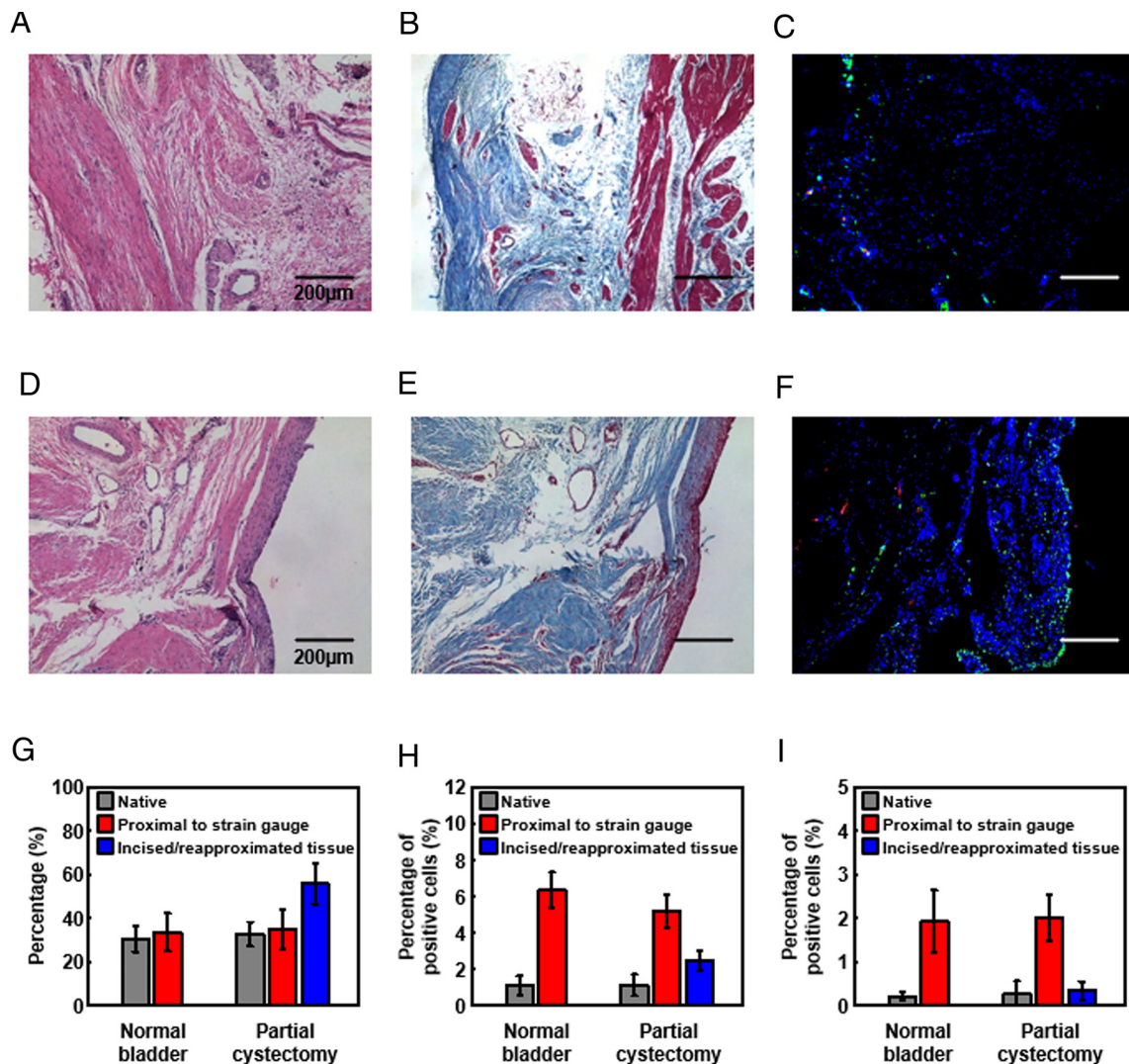


Fig. 6. Studies of biocompatibility of the wireless bladder monitoring system. Images for (A) H&E, (B) trichrome, and (C) M1/M2 inflammatory responses of bladder muscle near a strain gauge sutured onto the outer surface of a normal bladder. Images for (D) H&E, (E) trichrome, and (F) M1/M2 inflammatory responses of bladder muscle near a strain gauge sutured onto the outer surface of a bladder after a partial cystectomy. Quantitative histological evaluation of (G) collagen, (H) M1, and (I) M2 inflammatory responses for bladder muscle near strain gauges applied to a normal bladder and one with partial cystectomy.

In Vivo Biocompatibility in a Nonhuman Primate Model. Initial gross histological observations for the implanted strain gauge system at 10 wk postsurgery confirm an expected FBR surrounding the base station, most prominently at the suture locations and the wire leading to the strain gauge. A modest FBR appears around the strain gauge integrated onto the bladder surface. Histological analysis reveals biocompatibility on H&E, trichrome, proinflammatory marker (M1 macrophage, CD86), and anti-inflammatory marker (M2 macrophage, CD206) inflammatory responses in bladder muscles near the strain gauge. Fig. 6 *A–F* shows the results for the normal bladder and the bladder with partial cystectomy, respectively. Fig. 6*G* indicates the collagen levels (a percentage of the collective total of collagen and muscle) to determine potential smooth muscle loss and excessive collagen formation after 10 wk postsurgery. In the case of the smooth muscle area that is distal to the strain gauge (native), the collagen levels for the normal bladder and the bladder with partial cystectomy are $31.0 \pm 6.0\%$ and $33.0 \pm 6.0\%$, respectively. In the case of the smooth muscle area proximal to the strain gauge, the collagen levels for the normal bladder and the bladder with partial cystectomy are $34.0 \pm 9.0\%$ and $35.0 \pm 9.0\%$, respectively. Observations indicate no apparent differences in collagen levels in the muscle layer distal and proximal to the strain gauge ($P < 0.5$). The only apparent difference is the collagen level ($56.0 \pm 9.0\%$) in the smooth muscle area of the incised/reapproximated tissue in the baboon with partial cystectomy, as might be expected due to the cystectomy procedure and ensuing response. Fig. 6 *H* and *I* shows the results of immunofluorescence staining to monitor the presence of M1 and M2 macrophages, respectively, to statistically analyze the normal and partially cystectomized bladder. Native muscle areas of both baboons (normal bladder and bladder with partial cystectomy) have an M1 level of less than 1.1% and an M2 level of less than 0.5%. In contrast, the M1 levels in the muscle areas proximal to the strain gauge are $6 \pm 1\%$ and $5 \pm 1\%$ for the normal bladder and the bladder with partial cystectomy, respectively. The M2 levels for both cases are under 2%. The muscle area of the incised/reapproximated tissue in the baboon with partial cystectomy has an M1 level of $2.5 \pm 0.6\%$ and an M2 level of $0.3 \pm 0.2\%$. Overall, M1 and M2 levels are relatively low in the muscle area proximal to the strain gauge for both baboons. These results demonstrate that the inflammatory response to the strain gauge is low.

Discussion

This study introduces a wireless, implantable system for remote and real-time bladder monitoring, with examples that integrate at single or multiple locations on the outer wall of the bladder. The data confirm negligible effect on natural bladder activity due to the thin geometries and low mechanical moduli of the strain gauges, available in both permanent and bioresorbable forms. The technology thus has characteristics for envisioned uses in diagnosing and managing long-term recovery of bladder function for patients who have undergone partial cystectomies as treatment for bladder-related dysfunction. The application of multiple gauges can provide data corroboration from unique bladder locales where bladder tissue homogeneity may be in question due to insult or during a regenerative phase. As a specific example, one strain gauge can be applied to monitor the degree of recovery of a normal bladder or a bladder that has undergone partial cystectomy. Alternatively, when suturing the scaffold for bladder regeneration after partial cystectomy, two strain gauges can be applied to the scaffold and the normal bladder respectively, allowing the degree of bladder recovery to be monitored by comparing normal and regenerated bladder tissue on the scaffold. Compared to traditional urodynamics, which only provide a glimpse into bladder function

at a single point in time, this bladder monitoring system can inform physicians or patients of indications of bladder dysfunction or other side effects, in a remote fashion to enable early intervention. Experimental studies and computational modeling of bladder function in phantom constructs and in rat and nonhuman primate models that simulate injury/recovery verify the capabilities and highlight key engineering design features. Specific results validate the accuracy of the measurements in vivo and illustrate our ability to track bladder pressure for up to 8 wk in nonhuman primate models with both normal and partially cystectomized bladders, without adverse effects or detrimental inflammatory responses. To avoid the need for a secondary surgery to remove the device after monitoring for a required period, the PCB, electronic components, and battery for data measurement and wireless data transmission must be converted to bioresorbable formats using previously reported schemes in bioresorbable electronics. The technologies introduced here may have broader applications as permanent or temporary implants to monitor recovery processes after invasive surgeries, for improved patient care and optimized procedures and rehabilitation strategies.

Materials and Methods

Fabrication of the Bladder Monitoring System. The fabrication process for the strain gauge involved attaching a polyvinyl-alcohol (PVA) film (50 μm , Ruimao) on a glass substrate (1 mm, Fisher brand) with PI tape (KPT-1/4, Bertech), spin-coating a silicone elastomer (Ecoflex 00-30, Smooth-On) at 2,000 rpm for 30 s, attaching a Cu/PI (9 $\mu\text{m}/12 \mu\text{m}$) electrode, and annealing on a hot plate at 110 °C for 60 s. After screen-printing a carbon black (Vulcan XC 72R, Fuel Cell Store) doped silicone elastomer (22.5 wt%) through a PI mask (75 μm , American Durafilm) and curing on a hot plate at 110 °C for 5 h, the connection between the carbon black doped silicone elastomer and Cu/PI electrode was exposed to a corona discharge (1.5 kV, MultiDyne M1000-261, 3DT). A mask of PDMS (thickness ~ 1 mm) covered the Cu/PI electrode in preparation for spin-coating a silicone elastomer at 2,000 rpm for 30 s and curing on a hot plate at 110 °C for 60 s. An ultraviolet laser prototyping system (LPKF Laser & Electronics) cut the outline of the strain gauge. Helical coil wires (SCL-0.7, Open Source Instruments) connected the strain gauge and base station by soldering to the Cu/PI electrode and the PCB, respectively. Casting a layer of silicone elastomer on the soldered regions and curing on a hot plate at 110 °C for 60 s formed an encapsulating structure. As a final step, immersion in deionized (DI) water dissolved the PVA film.

The base station used a PCB (PCBWay) populated with electronic components, including a lithium-ion battery (LP501218, 1578, DigiKey) and an interconnecting wire, using a low-temperature reflow process with soldering paste (TS391LT, Chip Quik) and heat gun (AOYUE Int866). The encapsulation process involved coating parylene, marine epoxy (1919324, Loctite), and PDMS (Sylgard 184, Dow Corning) three times. To prevent disconnection of the helical coil wire, a mold with a design that forms a conical-shaped encapsulation at the connection between the base station and the helical coil wire was used. After placing the base station in the mold, silicone elastomer was poured and annealed at 75 °C for 1 h. An ethylene oxide (EtO) sterilization process disinfected the entire system prior to implantation.

Fabrication of the Bioresorbable Strain Gauge. The process of synthesizing the POMaC involved mixing 4.08 g maleic anhydride (800408, Sigma-Aldrich), 12 g citric acid (251275, Sigma-Aldrich), and 15.22 g 1,8-octanediol (A1540214, Alfa Aesar) in a three-necked round-bottom flask, stirring under a nitrogen atmosphere, and annealing at an initial temperature of 160 °C. After the mixture melted and became a clear liquid solution, the temperature was set to 140 °C, and the mixture was continuously stirred for 2 h. Dissolving the resulting viscous prepolymer in 80 mL ethanol (07-678-007, Fisher Scientific) with 5 wt% photoinitiator (Irgacure 2959, Sigma-Aldrich) allowed for UV curing in a PTFE dish (S29215, Fisher Scientific) for 5 h. Mixing the POMaC solution and W particles with 100 wt%. After mixing the W (GF40843245, Sigma-Aldrich) particles and POMaC solution at 100 wt% and screen-printing this composite on a film of POMaC through a PI

mask, prepared this material for UV curing for 2 h. An ultraviolet laser prototyping system defines the outline of the POMaC film with the W doped POMaC. W wires (50 μm) inserted into the W doped POMaC served as an electrical interconnect. The top POMaC layer overlapped the bottom POMaC film with the W doped POMaC, with bonding by heating at 200 $^{\circ}\text{C}$ for 30 s.

Strain Gauge Implantation for the Rodent Model. Athymic nude rats (females weighing \sim 200 g; 9 to 10 wk of age; Charles River Laboratories) were anesthetized with inhalation of 2% isoflurane. A 3.0 cm midline incision was made, and the abdominal wall musculature was exposed with subsequent identification of the urinary bladder. The base station of the device was sutured to the internal abdominal wall at two points using a 4-0 polydioxanone suture. At this point, the bladder was filled to approximately 50% capacity with sterile saline, and the device's wire was attached to the superficial portion of the bladder with a 7-0 polydioxanone suture at two points to stabilize the wire to the bladder. The strain gauge was then connected to the bladder at three points to the anterior portion of the bladder. Finally, the strain gauge was wrapped around the bladder and secured at a single point on the posterior portion of the bladder.

Rodent Tissue Processing. Bladder tissue was processed by dissecting the whole bladder and kidneys, fixed in 4% paraformaldehyde, and fully processed into paraffin wax molds, with tissue sections cut to 5 μm and placed on glass slides as previously described (26).

Rodent Histological Analysis and Immunostaining. H&E staining was completed as previously described (26, 27). Tissue sections underwent further evaluation through immunohistochemistry staining. With the use of inflammatory markers CD68 and MPO with a concentration of 3 to 4 $\mu\text{g}/\text{mL}$ (Abcam). Secondary antibodies ranged from 2 to 4 $\mu\text{g}/\text{mL}$ (Invitrogen) with DAPI nuclei staining.

Quantitative Histological Evaluation for the Rodent Model. H&E tissue evaluation was performed with 10 \times magnification of the strain gauge implanted area. Immunofluorescent quantification involved assessing $n = 5$, 10 \times images of the implanted strain gauge area per animal and utilizing the same ImageJ function as previously described (26, 27).

Strain Gauge Implantation and Urodynamics for the Nonhuman Primate Model. Anesthesia of baboons (*Papio anubis*; female; 7 to 10 kg; 2 to 4 y in age) consisted of ketamine (10 mg/kg, IM) for sedation and propofol (2 to 4 mg/kg, IV to effect) for endotracheal intubation. Hydromorphone (0.1 mg/kg, IV), extended-release meloxicam (0.6 mg/kg, SQ, once), and cefazolin (25 mg/kg, IV) were given preoperatively for analgesia and antibiotic prophylaxis. General anesthesia was maintained using inhalational isoflurane (0.5 to 1%), with continuous cardiopulmonary monitoring performed by veterinary staff. Extended-release buprenorphine (0.2 mg/kg, SQ, once) was given for postoperative analgesia. A 10-French foley catheter was placed using a sterile technique. Following adequate anesthesia, the bladder was fully drained. After initial bladder and renal ultrasound imaging (Sonosite M Turbo FUJIFILM SonoSite), images of the kidney were taken in a transverse and longitudinal fashion in gray scale and with Doppler. For UDS, the foley catheter was connected to a physiological pressure transducer (SP844, MEMSCAP) and an instillation pump (11 Elite Syringe Pump-Harvard Apparatus). A 25/75 CystoConray contrast solution and sterile saline filled the bladder at a rate of 10% projected bladder capacity per minute. The foley catheter connected to a transducer and bridge amplifier (Model FE221; AD Instruments) recorded continuous tracings of the transvesical pressures using LabChart 7.3 Software (AD Instruments). C-arm fluoroscopy was used to obtain images intermittently throughout filling. Instillation of contrast solution was halted, and capacity was recorded when 20 cm H_2O intravesical pressure was achieved. A postfill set of ultrasound images and observations were completed evaluating the bladder, ureter, and kidneys. Subsequently, instilled sterile saline fills the bladder to 50% urodynamic capacity, and then, the foley catheter was capped. The abdomen was prepared with Betadine scrub and alcohol washed and draped. A vertical midline incision was made sharply, and dissection was carried through the fascia to the bladder. The base station of strain gauge system was implanted into the internal abdominal wall utilizing the four suture holes fabricated on the base station device using four nonabsorbable monofilament sutures (4-0 prolene). The implantation process of the strain gauge involved suturing the elastic portion of the strain gauge to the superficial portion of the bladder at five connection points

and suturing the wire to the bladder at two points to add extra support. One other baboon underwent an approximate 50% partial cystectomy using electrocautery, followed by the closure of the bladder with 4-0 Vicryl as described (20). To confirm the functionality of the strain gauge system, the inserted foley catheter infused the bladder with sterile saline prior to abdominal closure. The fascia was then closed in a running fashion using a 2-0 polydioxanone suture. 0.25% Bupivacaine was injected directly into the subcutaneous tissue. The abdominal wall was closed in layers, with Scarpa's fascia closed using 4-0 interrupted Vicryl, and 4-0 Vicryl as a subcuticular running skin closure. The strain gauge system monitored the postoperative bladder function postsurgery. Prior to killing, baboons were sedated with a treatment of ketamine and xylazine (10 mg/kg and 1 mg/kg, IM, respectively) to perform ultrasound, urodynamic study, and C-arm fluoroscopy as previously described. Killing was completed using pentobarbital IV overdose. The strain gauge device was then removed, followed by bladder, kidney, and ureter explantation. All animal procedures were completed in accordance with guidelines set forth and approved by the University of Illinois at Chicago Animal Care Committee (ACC) and the Northwestern University Institutional Animal Care and Use Committee (IACUC).

Nonhuman Primate Tissue Processing. Resected tissues were fixed in 4% paraformaldehyde for 24 h and then subjected to a tissue processing protocol utilizing an increasing percentage of ethanol solutions and finished with xylenes and paraffin washes. Following paraffin washes, paraffin wax molds were made, and samples were cut using an RM2125 RT microtome (Leica) to a 5 μm thickness and placed on glass slides (25).

Nonhuman Primate Tissue Histological Analysis and Immunostaining. Glass slides of sectioned tissue underwent Masson's trichrome staining (Sigma-Aldrich) to identify trilayer bladder architecture, followed by H&E to identify any inflammatory infiltration. Additional tissue sections underwent immunofluorescence staining with the following inflammatory markers to determine an inflammatory response to the strain gauge; M1 (CD86), M2 (CD206) with concentrations ranging from 2 to 4 $\mu\text{g}/\text{mL}$ (Abcam). Secondary antibodies ranged from 2 to 4 $\mu\text{g}/\text{mL}$ (Invitrogen). Immunohistochemistry was completed with DAPI to visualize nuclei and completed with Vectashield (Vector Laboratories) to prolong fluorescence (25).

Nonhuman Primate Tissue Quantitative Histological Analysis. Collagen and muscle levels were determined through microscopic imaging with a Nikon Eclipse 50i Microscope (Nikon Inc.) equipped with Spot Advanced Imaging Software (Diagnostic Instruments). Images were taken at 10 \times magnification with $n = 10$ images per animal of the respective tissue area (native, proximal to strain gauge, incised/re-approximated tissue) of each animal. Collagen and muscle percentages were evaluated utilizing (Adobe Systems Inc.). To amplify the difference between collagen (blue) and muscle (red) pixels, the magenta levels were increased twofold and cyan in the red/magenta spectra were reduced twofold. The histogram tool was then adjusted to 115% fuzziness and channels of red and blue pixels were selected individually per image. The collagen and muscle ratio were then calculated from these values. Inflammatory cell quantification was performed by evaluating $n = 5$, 10 \times images per appropriate tissue area and then manually counting positively stained inflammatory cells (through immunofluorescence methods) by utilizing the ImageJ cell counter plugin function (NIH). Total cell counts were performed by also using ImageJ software by adjusting the images to binary mode and then separating cells using the watershed function. The total cell count was then automatically counted with the analysis particle function (25–28).

FEM Simulations. The commercial software ABAQUS was used for FEM simulation of the strains during the expansion of the bladder following cystectomy, during recovery, and after complete recovery. The simulation involved two strain gauges attached to a hollow ellipsoid with eight-node 3D solid elements (C3D8RH). Refined mesh ensured accuracy, especially in the regions around the strain gauges. With the hydraulic fluid cavity, FEM simulation captured the process of fluid injection inside the bladder with a fluid density of 1,000 kg/m^3 and bulk modulus of 2 GPa. With a zero predefined temperature field, the relative volume change due to thermal expansion was $3\alpha\Delta T$, where α was the thermal expansion coefficient and ΔT was the temperature change. Temperature expansion simulated the volume change. ΔT was a virtual temperature change with no

unit, so it just reflected the volume change. To realize a five times fluid volume increase in experiments (50 mL to 300 mL), the settings of α and ΔT were 1 and 5/3, respectively. All materials use the Mooney–Rivlin hyperelastic model with a hardening coefficient of 0.25 and $D1 = 0$. The initial modulus of Ecoflex 00-50 (bladder), Ecoflex 00-30 (strain gauge), Dragon skin 10 (bladder undergoing the regeneration on the scaffold), and Dragon skin 20 (scaffold) was 260 kPa, 160 kPa, 330 kPa, and 400 kPa, respectively.

Data, Materials, and Software Availability. The main data supporting the results of this study are present in the paper and [SI Appendix](#).

ACKNOWLEDGMENTS. Support of this work was provided in part by the NIH National Institute of Diabetes and Digestive and Kidney Diseases [NIDDK; R01DK109539 (A.K.S.)] and the National Institute of Biomedical Imaging and Bioengineering [NIBIB; R01EB026572 (G.A.A., A.K.S., and J.A.R.)]. The content is solely the responsibility of the authors and does not necessarily represent the official views of the NIH. A.K.S. would like to acknowledge the Michelin Family and Legacy Healthcare for their generosity. K.K. acknowledges support from the National Research Foundation of Korea (NRF) grant funded by the Korea government (MSIP; Ministry of Science, ICT & Future Planning; No. 2021R1F1A106387111, No. 2022R1C1C1010555, No. 2020R1A5A8018367, and BK21). M.-H.S. acknowledges support by a grant from the Korea Health Technology R&D Project through the Korea Health Industry Development Institute (KHIDI), funded by the Ministry of Health and Welfare, Republic of Korea (grant number: HR20C0026).

Author affiliations: ^aQuerrey Simpson Institute for Bioelectronics, Northwestern University, Evanston, IL 60208; ^bSchool of Advanced Materials Science and Engineering, Sungkyunkwan University, Suwon 16419, Republic of Korea; ^cDivision of Pediatric Urology, Department of Surgery, Ann & Robert H. Lurie Children's Hospital of Chicago, Chicago, IL 60611; ^dStanley Manne Children's Research Institute, Louis A. Simpson and Kimberly K. Querrey Biomedical Research Center, Chicago, IL 60611; ^eSchool of Electrical Engineering, Korea Advanced Institute of Science and Technology, Daejeon 34141, Republic of Korea; ^fDepartment of Semiconductor Convergence Engineering, Sungkyunkwan University, Suwon 16417, Republic of Korea; ^gDepartment of Mechanical Engineering, Northwestern University, Evanston, IL 60208; ^hDepartment of Electrical and Computer Engineering, Sungkyunkwan University, Suwon 16419, Republic of Korea; ⁱDepartment of Information Convergence Engineering, Pusan National University, Yangsan 50612, Republic of Korea; ^jDepartment of Urology, Feinberg School of Medicine, Northwestern University, Chicago, IL 60611; ^kDepartment of Advanced Materials Engineering, Chung-Ang University, Anseong 17546, Republic of Korea; ^lDepartment of Electronic Engineering, Gachon University, Seongnam 13120, Republic of Korea; ^mBionics Research Center of Biomedical Research Division, Korea Institute of Science and Technology, Seoul 02792, Republic of Korea; ⁿBiologic Resources Laboratory, University of Illinois at Chicago, Chicago, IL 60612; ^oDepartment of Biomedical Engineering, Northwestern University, Evanston, IL 60208; ^pCenter for Advanced Regenerative Engineering, Northwestern University, Evanston, IL 60208; ^qDepartment of Surgery, Feinberg School of Medicine, Northwestern University, Chicago, IL 60611; ^rChemistry of Life Processes Institute, Northwestern University, Evanston, IL 60208; ^sInternational Institute for Nanotechnology, Evanston, IL 60208; ^tSimpson Querrey Institute for Bionanotechnology, Evanston, IL 60208; ^uSimpson Querrey Institute, Northwestern University, Chicago, IL 60611; ^vDepartment of Material Science and Engineering, Northwestern University, Evanston, IL 60208; and ^wDepartment of Neurological Surgery, Feinberg School of Medicine, Northwestern University, Chicago, IL 60611

Author contributions: J.K., M.I.B., K.K., G.A.A., A.K.S., and J.A.R. designed research; J.K., M.I.B., K.K., N.V.H., S.L., M.-H.S., Y.W., D.Y.P., J.W.K., S.R.M., J.L.C., J.H.L., S.K., H.R., K.Y., H.-J.Y., S.S.K., B.K., L.C.H., E.Y.C., and A.K.S. performed research; J.K., M.I.B., J.-Y.Y., H.-S.S., S.M.W., Y.H., G.A.A., and A.K.S. analyzed data; and J.K., M.I.B., M.K., G.A.A., A.K.S., and J.A.R. wrote the paper.

1. K.-E. Andersson, A. Arner, Urinary bladder contraction and relaxation: Physiology and pathophysiology. *Physiol. Rev.* **84**, 935–986 (2004).
2. N. Yoshimura, W. C. de Groat, Neural control of the lower urinary tract. *Int. J. Urol.* **4**, 111–125 (1997).
3. C. J. Fowler, D. Griffiths, W. C. de Groat, The neural control of micturition. *Nat. Rev. Neurosci.* **9**, 453–466 (2008).
4. J. M. Holzeierlein *et al.*, Partial cystectomy: A contemporary review of the memorial Sloan Kettering cancer center experience and recommendations for patient selection. *J. Urol.* **172**, 878–881 (2004).
5. B. K. Hollenbeck, D. A. Taub, R. L. Dunn, J. T. Wei, Quality of care: Partial cystectomy for bladder cancer—a case of inappropriate use? *J. Urol.* **174**, 1050–1054 (2005).
6. S. S. Chang *et al.*, Treatment of non-metastatic muscle-invasive bladder cancer: AUA/ASCO/ASTRO/SUO guideline. *J. Urol.* **198**, 552–559 (2017).
7. W. Kassouf *et al.*, Partial cystectomy for muscle invasive urothelial carcinoma of the bladder: A contemporary review of the M. D. Anderson Cancer Center experience. *J. Urol.* **175**, 2058–2062 (2006).
8. B. Abelson *et al.*, Ambulatory urodynamic monitoring: State of the art and future directions. *Nat. Rev. Urol.* **16**, 291–301 (2019).
9. R. A. Schmidt, Urodynamics simplified. *Urology* **37**, 449–454 (1991).
10. M. N. Dakurah, C. Koo, W. Choi, Y.-H. Joung, Implantable bladder sensors: A methodological review. *Int. NeuroUrol. J.* **19**, 133–141 (2015).
11. S. J. A. Majerus, S. L. Garverick, M. A. Suster, P. C. Fletter, M. S. Damaser, Wireless, ultra-low-power implantable sensor for chronic bladder pressure monitoring. *ACM J. Emerg. Technol. Comput. Syst.* **8**, 11 (2012).
12. S. J. A. Majerus *et al.*, Suburothelial bladder contraction detection with implanted pressure sensor. *PLoS One* **12**, e0168375 (2017).
13. B. T. Frainey *et al.*, First in human subjects testing of the uromonitor: A catheter-free wireless ambulatory bladder pressure monitor. *J. Urol.* **210**, 186–195 (2023).
14. Q. Wang, H.-B. Wang, H. Xu, W. Zhou, G.-Z. Liu, Noninvasive urination-desire sensing method based on bladder bioimpedance spectrum analysis. *J. Med. Biol. Eng.* **36**, 191–196 (2016).
15. L. Zhang *et al.*, A conformable phased-array ultrasound patch for bladder volume monitoring. *Nat. Electron.* **7**, 77–90 (2024).
16. A. D. Mickle *et al.*, A wireless closed-loop system for optogenetic peripheral neuromodulation. *Nature* **565**, 361–365 (2019).
17. C. A. Gutierrez, E. Meng, Low-cost carbon thick-film strain sensors for implantable applications. *J. Micromech. Microeng.* **20**, 095028 (2010).
18. N. Lu, C. Lu, S. Yang, J. Rogers, Highly sensitive skin-mountable strain gauges based entirely on elastomers. *Adv. Funct. Mater.* **22**, 4044–4050 (2012).
19. M. Montgomery *et al.*, Method for the fabrication of elastomeric polyester scaffolds for tissue engineering and minimally invasive delivery. *ACS Biomater. Sci. Eng.* **4**, 3691–3703 (2018).
20. B. L. Turner *et al.*, Biodegradable elastomeric circuit boards from citric acid-based polyesters. *NPJ Flex. Electron.* **7**, 25 (2023).
21. Y. Wu *et al.*, A sewing approach to the fabrication of eco/bioresorbable electronics. *Small* **19**, 2305017 (2023).
22. C. Fernandes, I. Taurino, Biodegradable molybdenum (Mo) and tungsten (W) devices: One step closer towards fully-transient biomedical implants. *Sensors* **22**, 3062 (2022).
23. S. Roccabianca, T. R. Bush, Understanding the mechanics of the bladder through experiments and theoretical models: Where we started and where we are heading. *Technology* **4**, 30–41 (2016).
24. J. Yang, A. R. Webb, G. A. Ameer, Novel citric acid-based biodegradable elastomers for tissue engineering. *Adv. Mater.* **16**, 511–516 (2004).
25. A. K. Sharma *et al.*, A nonhuman primate model for urinary bladder regeneration using autologous sources of bone marrow-derived mesenchymal stem cells. *Stem Cells* **29**, 241–250 (2011).
26. A. K. Sharma *et al.*, Cotransplantation with specific populations of spina bifida bone marrow stem/progenitor cells enhances urinary bladder regeneration. *Proc. Natl. Acad. Sci. U.S.A.* **110**, 4003–4008 (2013).
27. M. I. Bury *et al.*, The effects of bone marrow stem and progenitor cell seeding on urinary bladder tissue regeneration. *Sci. Rep.* **11**, 2322 (2021).
28. M. I. Bury *et al.*, Multipotent bone marrow cell-seeded polymeric composites drive long-term, definitive urinary bladder tissue regeneration. *Proc. Natl. Acad. Sci. U.S.A. Nexus* **3**, pgae038 (2024), 10.1093/pnasnexus/pgae038.